Bessel Function Model of the Electron Pressure Profile Normalized by Gyro-Bohm Type Parameter Dependence

Junichi MIYAZAWA, Tomohiro MORISAKI, Motoshi GOTO, Ryuichi SAKAMOTO, Gen MOTOJIMA, Masahiro KOBAYASHI, Kiyomasa WATANABE, Hisamichi FUNABA, Ichihiro YAMADA, Kenji TANAKA, Akiyoshi MURAKAMI, Hiroshi YAMADA, and LHD Experiment Group

National Institute for Fusion Science, 322-6 Oroshi, Toki, Gifu 509-5292, Japan

(Received: 4 November 2009 / Accepted: 8 March 2010)

A model of electron pressure profile named gyro-Bohm normalized Bessel function model (GB-BFM) has been proposed. GB-BFM is composed of a profile term given by zero-order Bessel function, which is based on the diffusive transport in cylindrical plasmas, and gyro-Bohm type parameter dependences on the density profile, the total heating power, and the magnetic field strength. Using GB-BFM, one can figure out the region where the transport is gyro-Bohm like and diffusive. GB-BFM has been applied to the experiments in LHD. Profile analysis of the plasmas with or without a large magnetic island induced by resonant magnetic perturbation coils has revealed that the gyro-Bohm like diffusion is prevailing in the plasmas independent of the existence of island, except for the edge region. The gyro-Bohm like and diffusive transport property is also recognized in the mantle region of high-density plasmas with an internal diffusion barrier, while the superdense core region is improved compared with GB-BFM.

Keywords: heliotron, energy confinement scaling, RMP, magnetic island, high-density, IDB, mantle

1. Introduction

Energy confinement times, τ_E, in magnetically confined plasmas have been intensively studied for many years. This time constant describes the conductive loss from the plasma as $P_L = W_p/\tau_E$, where W_p is the plasma stored energy that is proportional to both the density and temperature. In a fusion device, the sum of P_L and radiation loss is compensated by the heating power. It is therefore important to investigate the physics that determines τ_E, to predict the power balance in a future fusion reactor. Scaling laws of τ_E have been empirically derived. H-mode scalings for tokamaks [1,2] and international stellarator scalings (ISS) for helical plasmas [3,4] are the typical examples. These scalings usually consist of both device parameters and operational parameters. Once the operational conditions including the heating power and averaged-density are given, these scalings can predict W_p and therefore the averaged-temperature in a device.

In a fusion reactor driven by alpha heating, however, the local temperature in the core region is more important than the averaged-temperature, since the thermo-nuclear fusion reaction mainly occurs in the high-temperature core region. As long as the radial profile of the temperature is known, as observed as stiffness in tokamaks [5,6], it is straightforward to estimate the core temperature from the averaged-temperature. However, this is not the case in helical plasmas where no strong stiffness has been observed [7-9], although the possible existence of a critical gradient has been suggested in W7-AS [6]. Therefore, a new kind of scaling law including the profile terms is highly desired especially for helical plasmas. Of course, it is desirable that this new scaling can also describe tokamak plasmas, for comprehensive understandings of magnetically confined plasmas.

In this study, a model of electron pressure profile in cylindrical plasmas is considered as a first step to construct a new scaling consisting of the profile terms. Details of the model are described in the next section. This model is then applied to the experiments in LHD [10]. Two kinds of neutral beam (NB) heated plasmas are chosen as typical examples; one is the plasma with a large magnetic island induced by resonant magnetic perturbation (RMP) coils [11,12] and another is the plasma with internal diffusion barrier (IDB) formed after intense hydrogen ice-pellet injection [13-15], which are described in Sections 3 and 4, respectively. Finally, a summary is given in Section 5.

2. Gyro-Bohm Normalized Bessel Function Model

2-1. Gyro-Bohm model

ISS95 [3] has been often referred to as a standard of the global energy confinement time in helical plasma experiments. This has been updated to ISS04 with new data from LHD and other devices [4]. ISS04 is called a gyro-Bohm like scaling, since its non-dimensional form is approximately proportional to τ_{Bohm}/ρ_*, where τ_{Bohm} is the

author's e-mail: miyazawa@LHD.nifs.ac.jp

Bohm confinement time and $\rho_* = \rho_i/a$ is the ion gyro-radius normalized to the plasma minor radius. Similar gyro-Bohm like dependence is also recognized in ISS95 and tokamak H-mode scalings [7]. The gyro-Bohm model is based on the drift-turbulence models, where the micro turbulence that drives anomalous transport has a scale length of the order of ρ_i with a decorrelation time of the order of ion diamagnetic drift time [16-19]. The thermal diffusivity in the gyro-Bohm model is given by $\chi_{GB} \propto T^{1.5} / (a\, B^2)$, where T is the temperature and B is the magnetic field strength. Using a relation of $W_p \propto a^2\, R\ \bar{n}_e\, T \propto P_H\, \tau_E$ (*i.e.*, $T \propto P_H\, \tau_E\, a^{-2}\, R^{-1}\ \bar{n}_e^{-1}$), the pure gyro-Bohm scaling, $\tau_{GB} \propto a^2 / \chi_{GB} \propto a^3\, B^2\, T^{-1.5} \propto a^3\, B^2\, (P_H\, \tau_E\, a^{-2}\, R^{-1}\, \bar{n}_e^{-1})^{-1.5}$ (*i.e.*, $\tau_{GB}^{2.5} \propto a^6\, R^{1.5}\, P_H^{-1.5}\, \bar{n}_e^{1.5}\, B^2$), is given by

$$\tau_{GB} \propto a^{2.4}\, R^{0.6}\, P_H^{-0.6}\ \bar{n}_e^{0.6}\, B^{0.8}, \tag{1}$$

where R, P_H, and $\bar{n}_e$ denote the plasma major radius, the heating power, and the line-averaged electron density, respectively.

2-2. Bessel function model

Here, let us consider a model of energy profile, $\varepsilon(\rho)$, where ρ is the normalized minor radius defined by the square-root of the toroidal flux normalized so as to give $\rho = 1$ at the last-closed-flux-surface (LCFS), in cylindrical plasma as an approximation of high-aspect ratio toroidal plasma. Volume integration of $\varepsilon(\rho)$ gives W_p (*i.e.*, $\int_0^1 \varepsilon(\rho)(dV/d\rho)d\rho = W_p$). Note that $\varepsilon(\rho)$ is proportional to the pressure profile that is the product of density and temperature, *i.e.*, $\varepsilon(\rho) \propto p(\rho) \propto n(\rho)\, T(\rho)$. Assume that $\varepsilon(\rho)$ self-similarly decays with a time constant of τ, *i.e.*, $\varepsilon(\rho, t) = \varepsilon(\rho) \exp(-t/\tau)$. The energy flux is given by $\Gamma = -\chi \nabla\varepsilon$, where the diffusivity χ is assumed to be independent of ρ. It should be noted that the Γ in this model is composed of the energy fluxes driven by both the temperature and density gradients. Therefore, the χ here does not necessarily equal to the conventional thermal diffusivity, which is related to the temperature gradient alone. The continuity equation is given by $\partial\varepsilon/\partial t = -\nabla\cdot\Gamma$, that can be transformed to $(-1/\tau)\, \varepsilon(\rho) = \chi \nabla^2 \Gamma$, and

$$\frac{1}{r}\frac{\partial}{\partial r}\left(r\frac{\partial \varepsilon}{\partial r}\right) + \frac{1}{\chi\tau}\varepsilon = 0\,. \tag{2}$$

The solution of Eq. (2) is given by zero-order Bessel function, J_0, as below;

$$\begin{aligned}\varepsilon(\rho, t) &= \varepsilon_0\, J_0(r/(\chi\tau)^{0.5}) \exp(-t/\tau),\\ &= \varepsilon_0\, J_0(2.4\,\rho) \exp(-t/\tau),\end{aligned} \tag{3}$$

where ε_0 is the central value of the energy profile that will be determined by the experiment. Note that no convection is assumed in this model and therefore the transport is fully *diffusive*. Also note that the steady-state solution with a heating profile proportional to $\varepsilon(\rho)$, *i.e.*, $P_H(\rho) \propto \varepsilon(\rho) \propto J_0(2.4\,\rho)$, also has a radial profile proportional to J_0.

2-3. Gyro-Bohm normalized Bessel function model

According to the discussion above, the pressure profile in cylindrical plasmas, or high-aspect ratio toroidal plasmas, is proportional to J_0, as long as the transport coefficient is independent of ρ. Assuming the gyro-Bohm type parameter dependence as in Eq. (1) and constant electron density of $n_e(\rho) = n$, the electron pressure profile, $p_e(\rho)$ ($\propto \tau_{GB}\, P_H$) can be modeled by

$$p_e(\rho) = C\ n^{0.6}\ P_H^{0.4}\ B^{0.8}\ J_0(2.4\rho), \tag{4}$$

where C is a constant. In the experiments, however, the density profile is not a constant. To include this effect, we assume that the local electron pressure at $\rho = \rho_1$ is expressed by substituting the local electron density $n_e(\rho_1)$ for n, *i.e.*,

$$p_e(\rho_1) = C\ n_e(\rho_1)^{0.6}\ P_H^{0.4}\ B^{0.8}\ J_0(2.4\rho_1). \tag{5}$$

Extending this to the whole radial position, we define the gyro-Bohm normalized Bessel function model (GB-BFM) of pressure profile, $p_{GB\text{-}BFM}(\rho)$ as below;

$$p_{GB\text{-}BFM}(\rho) = C\ n_e(\rho)^{0.6}\ P_H^{0.4}\ B^{0.8}\ J_0(2.4\rho/\alpha), \tag{6}$$

where $\alpha = a_{J0=0}/a_{LCFS}$ is introduced to explicitly include the experimental observation that the radial position, $a_{J0=0}$, where the pressure becomes zero is ordinarily different

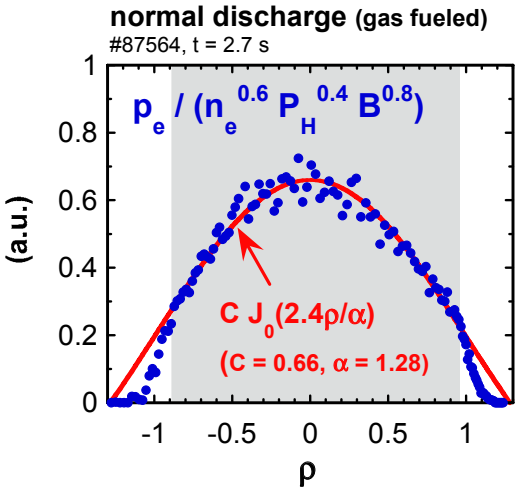

Fig.1 Typical radial profile of gyro-Bohm normalized electron pressure in a density ramp up discharge fueled by gas puffing (see Figs. 2 and 4). The result of least-square fitting to zero-order Bessel function is also shown. In the shaded region, the electron pressure profile is well reproduced by GB-BFM.

from the radial position of LCFS, a_{LCFS}.

In the following sections, we use $P_{GB\text{-}BFM}(\rho)$ to fit the electron pressure profiles measured by Thomson scattering [20]. The constants C and α are determined by the least-square method to fit the pressure data at $0 < \rho < \rho_{max}$ to the model, where ρ_{max} is also optimized to give the minimum of chi-square. The equilibrium used for data mapping, which is chosen from a database calculated by VMEC code [21], is also optimized in the fitting procedure. In some cases, we will compare the gyro-Bohm normalized pressure profile, $p_e(\rho)/(n_e(\rho)^{0.6}\ P_H^{0.4}\ B^{0.8})$, and C $J_0(2.4\rho/\alpha)$, instead of comparing $p_e(\rho)$ and $P_{GB\text{-}BFM}(\rho)$. A typical example of fitting result is shown in Fig. 1, where the gyro-Bohm normalized electron pressure profile in a density ramp-up discharge fueled by gas puffing is compared with the best fit of C $J_0(2.4\rho/\alpha)$. This discharge will be discussed again in the next section. As is seen in the figure, our model can fit the electron pressure profile inside $\rho \sim 0.9$. In other words, the transport in this region is gyro-Bohm like and diffusive. In the edge region of $\rho \sim 1$, however, our model fails to reproduce the steep pressure gradient, *i.e.*, the transport in this region is non-gyro-Bohm and/or non-diffusive. This region is enlarged in the plasmas with a large magnetic island, as will be shown in the next section.

3. Impact of the Magnetic Island

In LHD, a large m/n = 1/1 and/or 2/1 magnetic island can be formed using RMP coils, where m and n denote the poloidal and toroidal mode number, respectively. Especially, the large m/n = 1/1 island formed in the edge region influences the global confinement. Typical density ramp-up discharges with (#87564) or without (#87559) a large m/n = 1/1 island are compared in Fig. 2. The RMP coils were activated throughout the discharge duration in #87559. The diamagnetic plasma stored energy, W_p, is largely reduced in the discharge with the island (#87559), compared with the normal discharge (#87564) at similar NB heating power, P_{NB}. Nevertheless, the central electron density, n_{e0}, and pressure, p_{e0}, are similar for these two discharges.

According to the gyro-Bohm model, or the international stellarator scalings, $W_p = P_H\ \tau_E$ is expected to be proportional to $\bar{n}_e^{\ 0.6}$ (see Eq. (1)). This relation is also recognized in the experiment. In Fig. 3(left), W_p in four

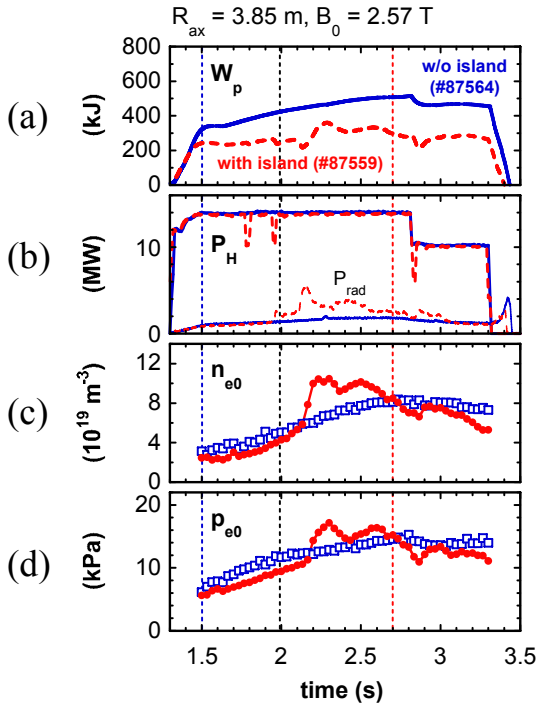

Fig.2 Waveforms in density ramp-up discharges fueled by gas puffing with (#87559, broken lines or closed circles) or without (#87564, solid lines or open squares) a large m/n = 1/1 magnetic island. (a) The diamagnetic plasma stored energy, W_p, (b) the NB heating power, P_H (and the radiation loss, P_{rad}), (c) the central electron density, n_{e0}, and (d) the central electron pressure, p_{e0}, are shown.

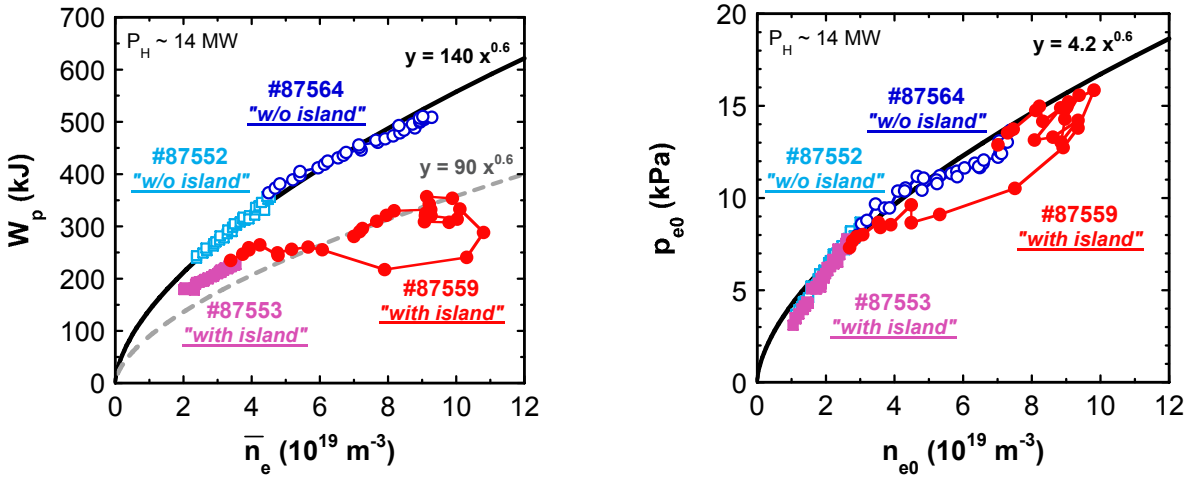

Fig.3 (left) The plasma stored energy dependence on the line-averaged electron density, and (right) the central electron pressure dependence on the central electron density, in discharges with or without the island.

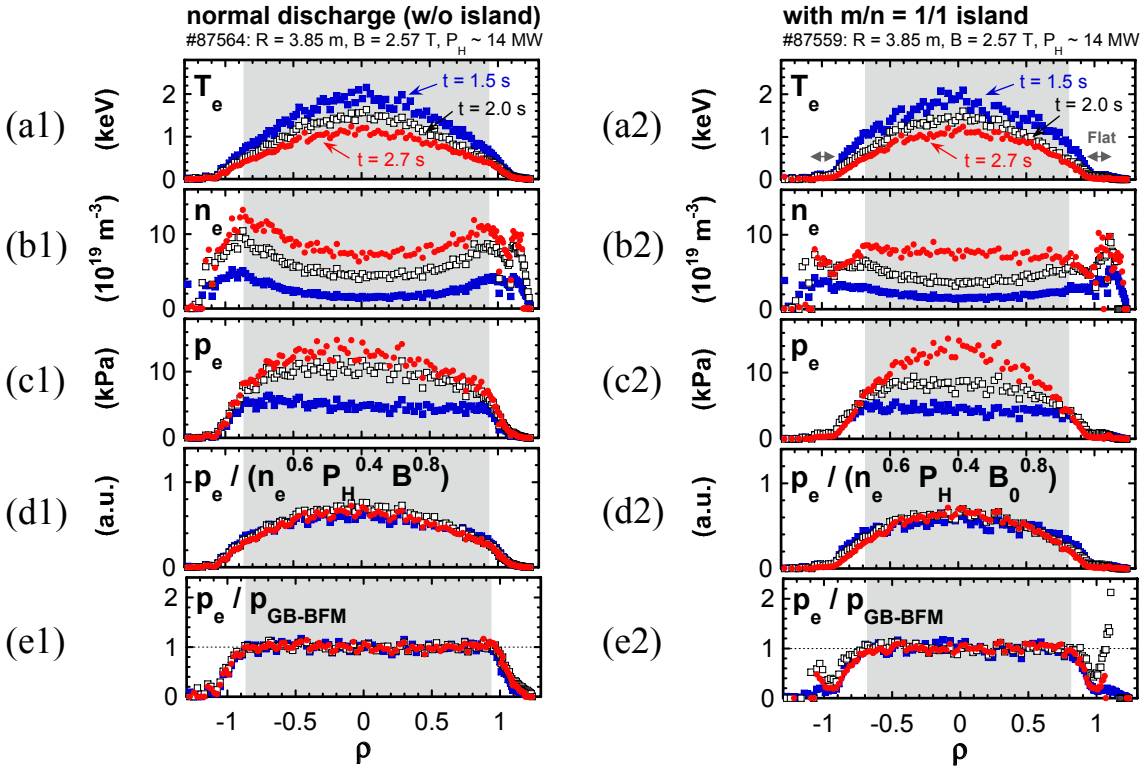

Fig.4 Radial profiles of (a1/a2) the electron temperature, (b1/b2) the electron density, (c1/c2) the electron pressure, (d1/d2) the gyro-Bohm normalized electron pressure, $p_e(\rho)/(n_e(\rho)^{0.6} P_H^{0.4} B^{0.8})$, and (e1/e2) the ratio of $p_e(\rho)$ to the fitting result of $p_{GB\text{-}BFM}(\rho)$, in the normal discharge without island (#87654, left column) and the discharge with the island (#87559, right column). In the shaded regions, the p_e profiles are well reproduced by the GB-BFM.

discharges with or without the island are plotted with respect to $\bar{n}_e$. In the normal discharges without island, W_p is proportional to $\bar{n}_e^{0.6}$. Similar density dependence is also recognized in the discharges with the island, although the proportional coefficient decreases from 140 to 90. As will be discussed later on, this confinement degradation can be attributed to the shrinkage of confinement region due to the large island. Even though the global confinement is degraded, the central pressure is not influenced by the island as shown in Fig. 3(right), where p_{e0} in the same discharges as shown in Fig. 3(left) is plotted with respect to n_{e0}. In this case, p_{e0} in these four discharges shows similar density dependence of $p_{e0} \sim 4.3\ n_{e0}^{0.6}$, *i.e.*, the gyro-Bohm like density dependence is also recognized in the relation between the local central electron pressure and the local central electron density.

As seen in Fig. 3, both the plasma stored energy and central pressure show gyro-Bohm like density dependence, while the response to the large magnetic island is different. To explain this, radial profiles of the electron temperature, density, and pressure are compared in Fig. 4, together with the gyro-Bohm normalized pressure profile of $p_e(\rho)/(n_e(\rho)^{0.6} P_H^{0.4} B^{0.8})$ and the ratio of $p_e(\rho)$ to the fitting result of $p_{GB\text{-}BFM}(\rho)$ introduced in Section 2. In the normal discharge without island (left column in Fig. 4), the temperature profile is expanding slightly outside the LCFS ($\rho = 1$). The density profile is hollow and its peak locates around $\rho \sim 0.9$. The density gradient at $0.9 < \rho < 1.0$ suggests an existence of inward particle convection, since the temperature in this region is so high (200 – 600 eV) that the particle source due to the ionization of light ion species is negligible.

In the discharge with the $m/n = 1/1$ magnetic island (right column in Fig. 4), on the other hand, flattening of the temperature profile due to the island is recognized in the edge region of $\rho \sim 1$, where the $\iota = 1$ surface exists in this magnetic configuration ($\iota = \iota/(2\pi) = 1/q$ is the rotational transform and q is the safety factor). The edge density decreases in this case. The magnetic island is intersecting the LCFS and therefore connecting the confinement region and the region outside the LFCS called stochastic layer. Although the mechanism is not fully understood yet, this configuration enhances the particle transport in the edge region. The density peak observed at $\rho \sim 0.9$ in the normal discharge moves to $\rho \sim 0.7 – 0.8$ in the discharge with the island. The pressure profile shrinks due to the island, although the achieved central pressure is similar to that in the case without island. This shrinkage of pressure profile directly causes degradation in the global confinement.

The gyro-Bohm normalized pressure profile also shrinks due to the island. Nevertheless, the central value of this normalized pressure is not influenced by the existence

of the island. This is expected from the result shown in Fig. 3(right), where the gyro-Bohm like density dependence of the central pressure appears to be common for the discharges with and without the island. The region where this gyro-Bohm property is prevailing and the transport is diffusive is clearly shown in the bottom panels of Fig. 4, where radial profiles of the ratio of $p_e(\rho)/p_{GB\text{-}BFM}(\rho)$ are shown. The ratio is ~ 1, and therefore the transport is gyro-Bohm like and diffusive, at $\rho < 0.9$ in the normal discharge, and at $\rho < 0.7 - 0.8$ in the discharge with the island.

Summarizing, the magnetic island causes shrinkage of pressure profile and degradation in global confinement. The transport is gyro-Bohm like and diffusive inside $\rho <$ 0.9 and $\rho < 0.7 - 0.8$ in the normal discharge and the discharge with the island, respectively. This position corresponds to the peak position in the density profile. Outside this position, the transport is non-gyro-Bohm and/or non-diffusive. At least, the particle transport in this region is non-diffusive, since there is a density gradient without enough particle sources.

4. High-Density IDB Plasmas

Internal diffusion barrier (IDB) plasmas are formed after intense hydrogen ice-pellet injection and characterized by high central density, high central pressure, large Shafranov shift, and steep gradient in the core region [13-15]. Relatively low density in the peripheral region called the *mantle* [13] is favorable for achieving high-density, since the density limit in LHD is determined by the edge electron density at the LCFS, n_{ea} [22]. Independent of fueling method, achievable edge density is limited by a semi-empirically determined scaling called the Sudo density limit scaling, n_c^{Sudo}, which is proportional to the square-root of the heating power [23], *i.e.*,

$$n_{ea} < n_c^{Sudo}\ (10^{20}\ \mathrm{m^{-3}}) = 0.25\ \sqrt{\frac{P_H B}{a^2 R}}\,. \qquad (6)$$

When n_{ea} exceeds this limit, the hot plasma column begins to shrink. Then, one should stop further fueling; otherwise the plasma would collapse radiatively. A high-level of recycling can also cause radiative collapse of high-density plasmas near the density limit. On the other hand, one can increase the central density as long as the edge density is kept lower than n_c^{Sudo}. This has been demonstrated in the discharge shown in Fig. 5, where P_{NB} was reduced from 11 MW to 3 MW after IDB formation. In spite of a large reduction in the heating power, the condition of $n_{ea} < n_c^{Sudo}$ was satisfied and high-density plasma of the order of 10^{20} m^{-3} was sustained until the NB was stopped.

In Fig. 6 shown are the radial profiles of T_e, n_e, p_e, $p_e(r/a)/(n_e(r/a)^{0.6}\ P_H^{0.4}\ B^{0.8})$, and $p_e(r/a)/p_{GB\text{-}BFM}(r/a)$, at t = 1.9 s (during pellet injection (PI)), 2.3 s (IDB phase just after P_{NB} reduction), and 3.2 s (without IDB), in the

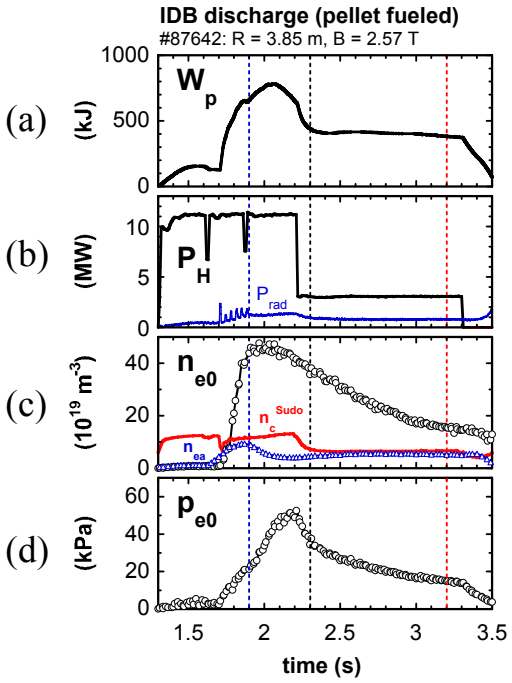

Fig.5 Waveforms in a pellet-fueled discharge with heating power reduction after IDB formation, where (a) the plasma stored energy, W_p, (b) the NB heating power, P_H (and the radiation loss, P_{rad}), (c) the central electron density, n_{e0} (together with the edge density at LCFS, n_{ea}, and the Sudo density limit, n_c^{Sudo}), and (d) the central electron pressure, p_{e0}, are shown from top to bottom.

discharge shown in Fig. 5. The superdense core region surrounded by IDB is obviously seen in the profiles of n_e and p_e at t = 2.3 s. Note that the abscissa is given by r/a in Fig. 6, for simplicity, since it is difficult to determine the equilibrium of IDB plasmas with high time resolution. The equilibrium of IDB plasmas with steep pressure gradient in the core region is still under investigation using HINT2 code [24]. Furthermore, the least-square method has been carried out to fit the pressure data at $0.5 < r/a < (r/a)_{max}$ to GB-BFM, to eliminate the data inside IDB.

In spite of the ambiguity in data mapping, the profile analysis using GB-BFM suggests important features of IDB plasmas. At first, the pressure profile at t = 3.2 s, which is well after pellet injection and therefore the IDB is lost completely, is well reproduced by the GB-BFM as seen in the bottom of Fig. 6. The transport property inside of $\rho < 0.9$ is gyro-Bohm like and diffusive, in this time slice. Secondly, according to the radial profile of $p_e(r/a)/p_{GB\text{-}BFM}(r/a)$ at t = 2.3 s, the mantle pressure is well reproduced by the GB-BFM, while the core pressure inside IDB is not. This means that the transport in the mantle region is gyro-Bohm like and diffusive, while it is improved inside IDB. Thirdly, the core confinement during pellet injection (t = 1.9 s) is deteriorated compared with

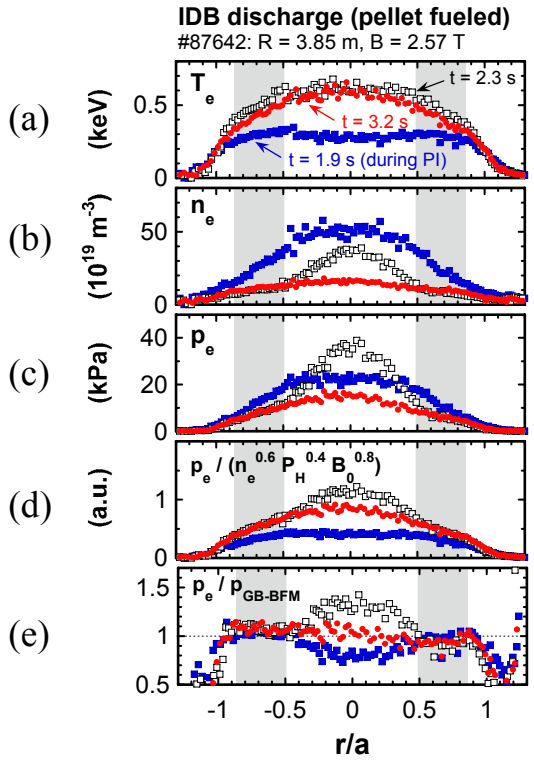

Fig.6 Radial profiles of (a) the electron temperature, (b) the electron density, (c) the electron pressure, (d) the gyro-Bohm normalized electron pressure, $p_e(r/a)/(n_e(r/a)^{0.6}P_H^{0.4}B^{0.8})$, and (e) the ratio of $p_e(r/a)$ to $p_{GB\text{-}BFM}(r/a)$, in the discharge shown in Fig. 5. The abscissa is given by r/a. The least-square method has been carried out to fit the pressure data at $0.5 < r/a < (r/a)_{max}$ to GB-BFM. The mantle region is shaded.

GB-BFM. This might be probably due to the lack of central heating power. At that time, the peripheral density is as high as $\sim 4 \times 10^{20}$ m^{-3} at $r/a \sim 0.5$. The high peripheral density prevents deep penetration of NB and the heat deposition moves from the core to periphery [25].

As was noted in Section 2 (below Eq. (3)), the GB-BFM is applicable to the plasmas with parabolic heat deposition profiles as $P_H(\rho) \sim J_0(2.4\rho)$. Therefore, lack of (or, excess of) central heating power compared with the parabolic heating profile can cause the deviation of pressure profile from GB-BFM. To reproduce the pressure profile with non-parabolic heating profile, it would be necessary to include the heat deposition profile, as the density profile, into the model.

5. Summary

A model of electron pressure profile (GB-BFM) has been constructed based on the diffusion in cylindrical plasmas with gyro-Bohm type parameter dependence. Then, it has been applied to the profile analysis on plasmas with a large magnetic island or IDB. In the analysis, the measured electron pressure profile has been fitted to the GB-BFM using the height and width of the pressure profile as fitting parameters of C and α, respectively. The equilibrium and fitting region are also optimized to minimize the chi-square.

Using GB-BFM, the followings have been clarified;

1) In normal plasmas fueled by gas-puffing, the transport inside the density peak around $\rho \sim 0.7 - 0.9$ is gyro-Bohm like and diffusive.
2) In the edge region of $\rho \sim 1$ (outside of the density peak), the transport is non-gyro-Bohm and/or non-diffusive.
3) A large magnetic island causes shrinking of the confinement region and degradation in the global confinement.
4) The energy transport in the mantle region of IDB plasmas is gyro-Bohm like and diffusive, as in gas-fueled plasmas.

To improve GB-BFM to reproduce the pressure profile in plasmas with non-parabolic heat deposition, it is necessary to include the heat deposition profile into the model.

Acknowledgements

This work is partly supported by NIFS09ULPP517.

[1] ITER Physics Basis Editors *et al.*, Nucl. Fusion **39**, 2137 (1999).
[2] Editors of 'Progress in the ITER Physics Basis' *et al.*, Nucl. Fusion **47**, S1 (2007).
[3] U. Stroth *et al.*, Nucl. Fusion **36**, 1063 (1996).
[4] H. Yamada *et al.*, Nucl. Fusion **45**, 1684 (2005).
[5] F. Ryter *et al.*, Phys. Rev. Lett. **86**, 5498 (2001).
[6] F. Ryter *et al.*, Plasma Phys. Control. Fusion **48**, B453 (2006).
[7] U. Stroth *et al.*, Plasma Phys. Control. Fusion **40**, 9 (1998).
[8] F. Wagner *et al.*, Plasma Phys. Control. Fusion **48**, A217 (2006).
[9] S. Inagaki *et al.*, Nucl. Fusion **46**, 133 (2006).
[10] A. Komori *et al.*, Nucl. Fusion **49**, 104015 (2009).
[11] A. Komori *et al.*, Nucl. Fusion **45**, 837 (2005).
[12] T. Morisaki *et al.*, J. Nucl. Mater. **337-339**, 154 (2005).
[13] N. Ohyabu *et al.*, Phys. Rev. Lett. **97**, 055002 (2006).
[14] H. Yamada *et al.*, Plasma Phys. Control. Fusion **49**, B487 (2007).
[15] R. Sakamoto *et al.*, Nucl. Fusion **49**, 085002 (2009).
[16] R.J. Goldston *et al.*, Bull. Am. Phys. Soc. **34**, 1964 (1989).
[17] F.W. Perkins, in *Heating in Toroidal Plasmas*, Rome, 1984 (International School of Plasma Physics, Varenna, 1984), Vol. 2, p.977.
[18] M. Murakami *et al.*, Phys. Fluids B **3**, 2261 (1991).
[19] J.G. Cordey *et al.*, Nucl. Fusion **39**, 301 (1999).
[20] I. Yamada *et al.*, Plasma Fusion Res. **2**, S1106-1 (2007).
[21] S.P. Hirshman, W. Van Rij and P. Merkel, Comput. Phys. Commun. **43**, 143 (1986).
[22] J. Miyazawa *et al.*, Nucl. Fusion **48**, 015003 (2008).
[23] S. Sudo *et al.*, Nucl. Fusion **30**, 11 (1990).
[24] Y. Suzuki *et al.*, Nucl. Fusion **46**, L1 (2006).
[25] H. Yamada *et al.*, Nucl. Fusion **43**, 749 (2003).